Interference Effects on Scattering by Parallel Fibers at Normal Incidence

Susan M. White* and Sunil Kumar†
NASA Ames Research Center, Moffett Field, California

This paper examines the radiative heat transfer through fibrous materials, focusing on the interactions between the scattered radiation from individual parallel fibers. A normally incident plane electromagnetic wave is considered, and different representative geometries are analyzed theoretically. Experimental results are presented for a specific case corresponding to fibers in one plane. The light-scattering characteristics of a single long fiber depend only on the size parameter and on the material optical constants. When multiple fibers are spaced closely together, the additional mechanism of interference between the scattered waves influences the scattering characteristics of the fiber assembly as a whole. Previous studies of radiative transport through fibrous media have ignored these effects. In this study analytical models are developed for obtaining the radiative scattering characteristics of fibrous media where the mechanism of interference is accounted for. The results indicate that interference decreases the scattering efficiency of fibrous media containing a large number of randomly positioned fibers. For other configurations the results are more complex. The predicted results are compared with experimental measurements of forward- and back-scattered light from a system of finite parallel fibers over a broad range of wavelengths.

Nomenclature

a = clearance between fibers, μm
A = scaled distance between fiber center, coplanar case
b = fiber cross-section area, mm^2
B = incident beam cross-section area, mm^2
c = clearance parameter, a/λ
d = fiber diameter, μm
e = unit vector
f_v = solid volume fraction
F = dependent scattering correction factor
g = scaled local fiber number density
I = intensity, W/m$^2 \cdot \mu$m $\cdot$ str
m = complex refractive index, $n + i\kappa$
n = index of refraction
N = number of fibers
Q = efficiency
r = position vector
R = scaled distance, r/d
Re = real part of complex number
S = scattered energy, %
T = transmittance, %
α = size parameter, $\pi d/\lambda$
κ = index of absorption
λ = wavelength, μm
Φ = scattering phase function
θ = angle from incident direction

Subscripts

a = absorption
back = backward hemisphere
e = extinction
for = forward hemisphere
i = from one individual fiber in independent scattering
j, k = fiber specifications
N = from N fibers
s = scattering
r = radial direction
x = along x axis (incident direction)
y = along y axis (normal to incident)

Presented as Paper 89-1717 at the AIAA 24th Thermophysics Conference, Buffalo, NY, June 12-14, 1989; received June 29, 1989; revision received Nov. 2, 1989.

*Research Scientist, Thermal Protection Materials Branch. Member AIAA.

†Thermal Protection Materials Branch, visiting from Department of Mechanical Engineering, University of California, Berkeley, CA; currently at Polytechnic University, Brooklyn, NY.

Introduction

HIGH-temperature ceramic fabrics are used as thermal insulation for atmospheric entry vehicles, including the Space Shuttle Orbiter component of the Space Transportation System (STS), and may be used on Aeroassisted Space Transfer Vehicles (ASTV).[1,2] These materials are blankets woven from ceramic fibers. Previous experimental work in this area[3] gave measurements in the ultraviolet/visible region for fabrics woven from silica yarns, from which bulk absorption and scattering coefficients were calculated using a two-flux scattering model. The present work presents new measurements on a different silica fiber configuration that preserves the essential geometry of the fabrics, extends the region of measurement to the infrared range of wavelengths for use in thermal radiation calculations, and, finally, puts a theoretical foundation under the experimental data. This is useful in feasibility studies for the design and evaluation of new materials, for example, to predict the thermal response of fabrics woven of smaller diameter fibers or of more closely or loosely packed yarns.

This study is motivated by the need to evaluate the radiation characteristics of ceramic fibrous systems that could be used in heat shielding on atmospheric entry vehicles where both convective and radiative heating may occur. The highly ordered, closely spaced parallel geometry of the fibers in a yarn or fabric affects the radiative transfer significantly by enhancing interference effects. Classical independent theory for studying such systems assumes that each fiber acts independently in the absorption and scattering of radiation, unaffected by the presence of other particles.[4] Departure from the assumption of the independent theory originates primarily from the mechanism of coherent addition (i.e., taking into account the constructive/destructive interference) of the far-field scattered radiation. These effects have been studied for systems containing small spherical particles, both analytically[5] and experimentally,[6] and for agglomerates of spherical particles.[7] Single

fibers[4,8] and fibrous insulations in the independent theory regime[9,10] have been extensively studied in the literature.

Analysis

Independent scattering theory is based on the assumption that the scattering from a collection of fibers can be obtained by algebraically summing up the scattering characteristics of each fiber. Each fiber is assumed to be uninfluenced by the presence of the other fibers; therefore the scattering from N identical fibers can be obtained by multiplying the scattering field from one fiber by N. There is always phase addition or cancellation of the scattered waves from different fibers, and the independent scattering assumption breaks down due to this mechanism when the fibers are closely spaced. This is the interference effect, which is mathematically expressed as

$$I_{sN}(\theta) = NI_{si}(\theta)\, F(\theta) \tag{1}$$

where I_s is the scattered intensity and θ is the angle between the forward scattering direction and the direction under consideration in the plane normal to the fiber. The correction factor used to account for the intereference effects is $F(\theta)$, which would equal unity if no interference effects were present, i.e., if the independent scattering assumption were valid. Both the correction factor F and the intensity I depend on the size parameter $\alpha(=\pi d/\lambda)$ and the refractive index m of the fiber material, where $m = n + i\kappa$. The index of refraction and index of absorption depend on both the wavelength and the temperature. The correction factor F also is a function of the clearance parameter $c(=a/\lambda)$, where a is the clearance between fibers, as shown in Fig. 1. In order to simplify the notation, the dependence of F and I on wavelength λ, size parameter α, clearance c, and refractive index m are not indicated explicitly in the expressions given here. However they are considered during the evaluation of the intensity and the correction factor.

If the phase of the scattered waves is assumed to be proportional to the distance from the fiber centers, $F(\theta)$ is given by[5,7,11,12]

$$F(\theta) = \frac{1}{N}\,\mathrm{Re}\sum_{k=1}^{N}\sum_{j=1}^{N}\exp\left[i\frac{2\pi}{\lambda}(\boldsymbol{e}_x - \boldsymbol{e}_r)\cdot(\boldsymbol{r}_j - \boldsymbol{r}_k)\right] \tag{2}$$

where unit vector $\boldsymbol{e}_x$ is in the forward direction, $\boldsymbol{e}_r$ is the unit vector along the radial direction of observation and at an angle θ from the forward direction, and $\boldsymbol{r}_j$ and $\boldsymbol{r}_k$ the position vectors of the centers of the fibers j and k, as shown in Fig. 1. The dot product in the above equation represents the difference in the total distance traveled by the waves from a common origin to the detector after being scattered by fibers j and k. The above expression assumes that the change of phase across individual fibers is small and is thus most accurate for fibers of small size parameters. Because it accounts only for the phase interference and is thus independent of fiber properties, $F(\theta)$ is a geometric factor.

The scattering efficiency Q_s is the ratio of the total energy scattered by the fiber to the total energy intercepted by the fiber. The scattering efficiency is evaluated by integrating the scattered intensity over all angles. To mathematically isolate the effect of interference on the scattering efficiency, the ratio of this scattering efficiency to that of a single fiber is presented as follows:

$$\frac{Q_{sN}}{Q_{si}} = \frac{1}{2\pi}\int_0^{2\pi}\Phi_i(\theta)F(\theta)d\theta \tag{3}$$

Here, Φ_i is the scattering phase function of an individual fiber and θ the angle between the scattered and incident directions. The phase function is evaluated by using the independent scattering theory and is a known function of the angle θ and the size parameter α. For small size parameters ($\alpha \ll 1$), the independent phase function asymptotes to

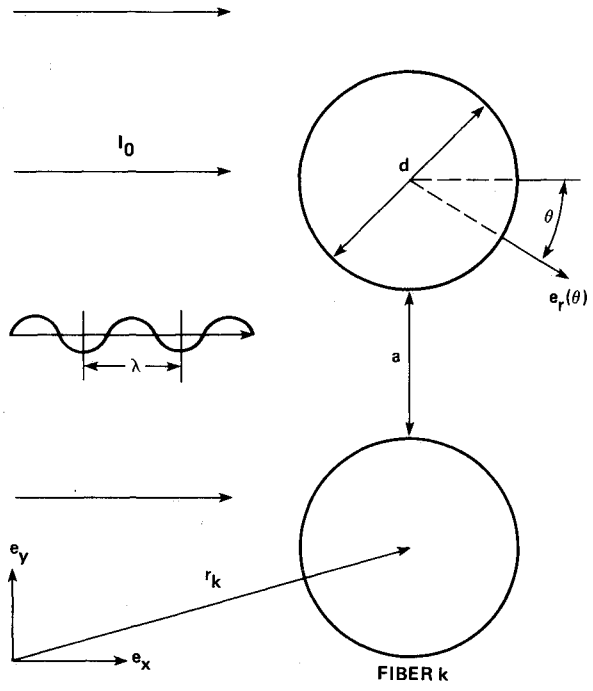

Fig. 1 Length scales and position vectors in the fiber system.

$$\Phi_i(\theta) = \frac{|m^2+1|^2 + 4\cos^2\theta}{|m^2+1|^2+2} \tag{4a}$$

$$= \frac{2}{3}(1+\cos^2\theta), \qquad m \approx 1 \tag{4b}$$

For larger size parameters the phase function is more complicated.

Evenly Spaced Coplanar Fibers

If a single plane layer containing N fibers spaced a fixed distance apart is subjected to incident electromagnetic radiation perpendicular to the layer, the following mathematical simplifications are applied. The y axis is positioned to run though the centers of the fibers and is normal to the fiber axes as well as the incident direction. When the index j equals k for each of the N fibers, the argument of the exponential function is zero; therefore that term in the summation becomes one and can be taken out from the summation. Thus $\boldsymbol{r}_j - \boldsymbol{r}_k$ is now proportional to $(j-k)\,\boldsymbol{e}_y$, the dot product reduces to a sine of the angle θ, and the form factor is written as

$$F(\theta) = 1 + \frac{1}{N}\,\mathrm{Re}\sum_{k=1}^{N}\sum_{\substack{j=1\\ j\neq k}}^{N}\exp\left[i\frac{2\pi}{\lambda}(\boldsymbol{e}_x - \boldsymbol{e}_r)\cdot(\boldsymbol{r}_j - \boldsymbol{r}_k)\right] \tag{5a}$$

$$= 1 + \frac{1}{N}\sum_{k=1}^{N}\sum_{\substack{j=1\\ j\neq k}}^{N}\cos\left[2\alpha A(k-j)\sin\theta\right] \tag{5b}$$

Here the ratio of the fixed distance between the centers of adjacent fibers to the diameter of the fibers is represented by $A\ (=1+a/d)$. Figure 2 shows the form factor $F(\theta)$ for 20 closely spaced fibers ($A = 1.05$), and the associated scattering efficiency is presented in Fig. 3. Figure 2 shows that $F(\theta)$ becomes more oscillatory as the size parameter α increases. For small α the scattered radiation from these closely spaced fibers always adds constructively since the different scattered

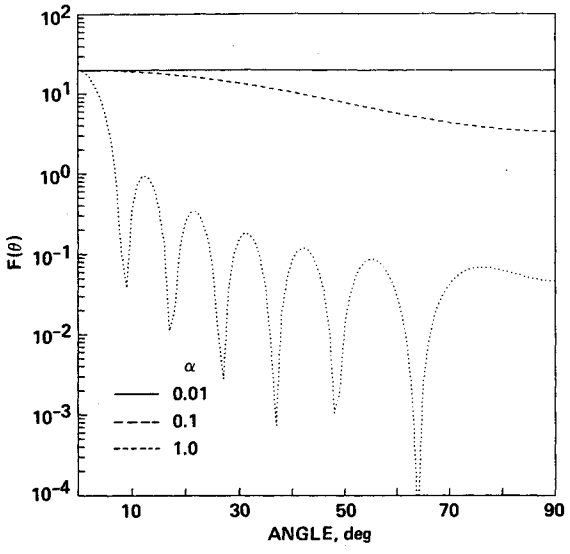

Fig. 2 The interference factor $F(\theta)$ for 20 coplanar, evenly spaced fibers, with clearance $c = 1.05$.

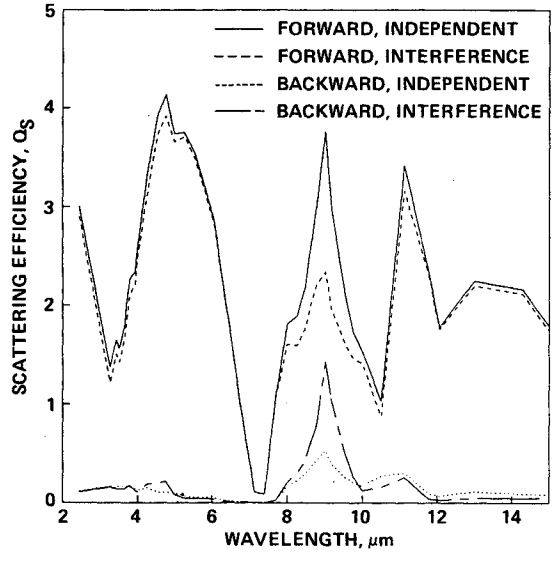

Fig. 3 The scattering efficiency for 20 coplanar fibers, refractive index $n = 1.55$, $A = 1.05$, $d = 9$ μm.

waves emanate from points that are very close to one another. The scattering efficiency shows a periodic variation with changing clearance. For small size parameters ($\alpha \ll 1$), the expression for scattering efficiency is readily integrated by using Eqs. (3), (4b), and (5b) as

$$\frac{Q_{sN}}{Q_{si}} = 1 + \frac{1}{N}\sum_{k=1}^{N}\sum_{\substack{j=1 \\ j\neq k}}^{N}\left\{J_0[2\alpha A(k-j)] + \frac{1}{3}J_2[2\alpha A(k-j)]\right\} \quad (6)$$

Randomly Positioned Fibers

Parallel fibers that are spaced in a random fashion are examined in this section. The random angular positions of the fibers relative to one another have the effect of simplifying the expression for the interference factor F. Fiber k is first considered fixed, and the angular positions of the jth fibers are averaged over all directions keeping the separation distances r_{jk} fixed. This yields[11,12]

$$F(\theta) = 1 + \frac{1}{N}\sum_{k=1}^{N}\sum_{\substack{j=1 \\ j\neq k}}^{N} J_0\left(4\alpha R_{jk}\sin\frac{\theta}{2}\right) \quad (7)$$

where J_0 is Bessel function of zeroth order and $R_{jk} = r_{jk}/d$.

The above expression is the first step for analyzing randomly positioned fibers, but it can also be utilized for examining systems containing a large number of fibers placed in a highly ordered close-packed pattern. Noting that in a large dense system, the effect of each fiber k in the above expression is identical except for the few fibers at the periphery of the system. However, these peripheral fibers are also assumed to have the same effect as those within the system. This approximation lets the summation over k be replaced by N, and the above can be then be expressed as follows

$$F(\theta) = 1 + \sum_{l=1}^{N-1} J_0\left(4\alpha R_l \sin\frac{\theta}{2}\right) \quad (8)$$

where R_l is the nondimensionalized radial distance from a representative fiber center to the center of the lth fiber centers around it. For example, with closely packed cylindrical systems where fibers are adjacent, each fiber in contact with exactly six nearest neighbors, may be analyzed by considering the central fiber as the representative fiber and $R_l = 1$ for $l = 1,\ldots, 6$ and so on.

More generally, the fibers are considered to be randomly distributed in space with the fiber separation given by a distribution function. The fibers are parallel to each other, and the above is then formalized as[11]

$$F(\theta) = 1 + 8f_v\int_0^\infty [g(R)-1]J_0\left(4\alpha R\sin\frac{\theta}{2}\right)R\,dR \quad (9)$$

where f_v is the solid volume fraction and $g(R)$ is the ratio of the local fiber number density at a distance R from the representative fiber to the average (bulk) number density. If the number density is assumed uniform for $r \geq d$ and is zero for smaller values of r, the above equation is readily integrated as

$$F(\theta) = 1 - \frac{8f_v}{4\alpha\sin\frac{\theta}{2}}J_1\left(4\alpha\sin\frac{\theta}{2}\right) \quad (10a)$$

$$= 1 - 4f_v\left[1 - \frac{1}{8}\left(4\alpha\sin\frac{\theta}{2}\right)^2\right], \quad \alpha \to 0 \quad (10b)$$

This particular form of the distribution function is more accurate for low volume fractions and breaks down as the packing becomes more dense. Figure 4 presents the results using this distribution [Eq. (10a)] and shows a reduction in scattering efficiency as the volume fraction increases. For small size parameters, the scattering efficiency is analytically obtained by integrating Eq. (3) using Eqs. (4b) and (10a) as

$$Q_{sN}/Q_{si} = 1 - 4f_v\left\{J_0^2(2\alpha) + J_1^2(2\alpha) + 1/3[J_2^2(2a) - J_1(2\alpha)\,J_3(2\alpha)]\right\} \quad (11)$$

For higher volume fractions, a modified distribution function that assigns additional solid volume near the fiber is considered. As before, the nondimensional number density $g(R)$ is assumed to be unity for $R > 1$. An additional delta

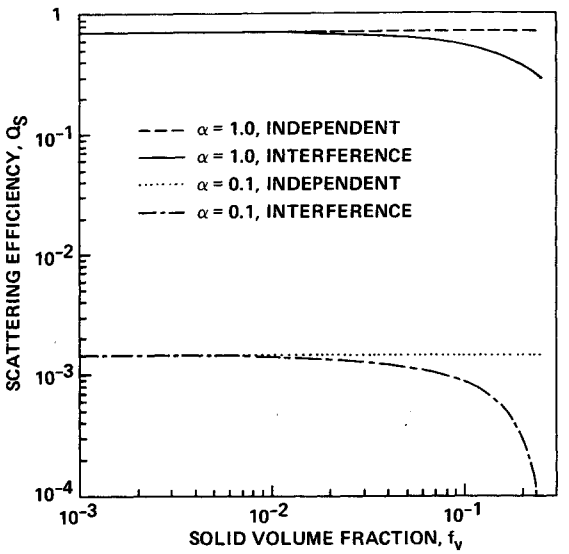

Fig. 4 The scattering efficiency for randomly packed fibers, with refractive index $n = 1.55$, $d = 9$ μm.

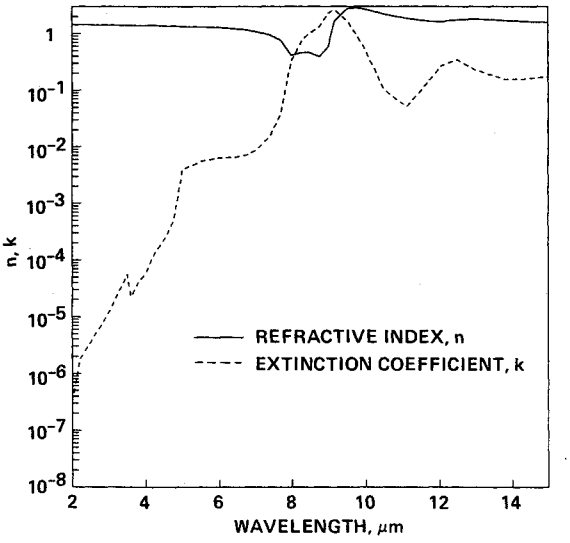

Fig. 5 The optical constants of silica at room temperature.

function at $R = 1$ is specified as[12]

$$\lim_{\delta \to 0} \int_{1-\delta}^{1+\delta} R_g(R)\, dR = \frac{1}{2}\left(1 - \frac{1}{2\pi}\right) = 0.4204 \qquad (12)$$

This distribution function yields

$$F(\theta) = 1 - \frac{8f_v}{4\alpha \sin\frac{\theta}{2}} J_1\left(4\alpha \sin\frac{\theta}{2}\right) + 8 \times 0.4204 f_v J_0\left(4\alpha \sin\frac{\theta}{2}\right) \qquad (13a)$$

$$1 - 4f_v\left[0.1592 + 0.0852\left(4\alpha \sin\frac{\theta}{2}\right)^2\right], \quad \alpha \to 0 \qquad (13b)$$

This [Eq. (13a)] is the expression used to compare with the experimental data, as discussed below. Using Eq. (13a) the following is obtained

$$Q_{sN}/Q_{si} = 1 - 4f_v\left\{J_0^2(2\alpha) + J_1^2(2\alpha) + 1/3\,[J_2^2(2\alpha) - J_1(2\alpha)\, J_3(2\alpha)]\right\} + 8 \times 0.4204 f_v\left[J_0^2(2\alpha) + (1/3)J_2^2(2\alpha)\right] \qquad (14)$$

Optical Constants

The optical properties of silica used were taken from Palik,[13] when possible, or were calculated from transmittance data from Touloukian and DeWitt[14] and from absorption coefficient data from Driscoll[15] and are shown in Fig. 5. The optical constants used in this analysis, the refractive index n and the extinction coefficient κ, were evaluated in high-absorption regions using the Kramers-Kronig analysis[13] of reflectance data whereas in regions of low absorption, transmission or absorption data and prism data were used.

Experimental Setup

The unique characteristic of a tightly woven ceramic fabric influencing interference effects on scattering from the individual fibers is the virtually parallel, highly ordered orientation of the fibers making up the yarns and, ultimately, the fabric. The stiffness of the ceramic fibers allows relatively little bending; therefore a typical fabric woven of these materials exhibits a basket-weave type of structure. The parallel orientation of the fibers reduces the scattering from a three-dimensional to a two-dimensional phenomenon, whereas the spacing between the fibers governs the phase lag resulting in interference at a given wavelength. The simplest configuration preserving these characteristics is a set of coplanar parallel fibers. The experimental specimen used in this work is an array of 60 parallel quartz fibers clamped at both ends in an aluminum sample holder. The fibers are 9 μm in diameter and 3.5 cm long. The sample holder suspends the fibers across a 3 cm port, which is wider than the diameter of the entrance or sample port of the integrating sphere.

Experimental measurements of the spectrally resolved reflectance and transmittance were made over the infrared region, from 2.5 to 15 μm, using a spectrophotometer equipped with an integrating sphere. The integrating sphere collects the light scattered into all angles of the forward or backward hemisphere depending on whether transmittance or reflectance measurements are being made on the sample. Reflections from the diffuse surface inside the integrating sphere average out the surviving angular components of the scattered or reflected radiation before it reaches the detector. To be specific, reflectance and transmittance measurements were made using a Bio-Rad Digilab FTS-40, a single-beam Fourier Transform Infrared Spectrophotometer (FTIR). It is equipped with a 4-in-diam integrating sphere manufactured by Labsphere with a diffuse gold internal coating. The FTIR is purged with nitrogen during use to reduce absorption by air at the water and carbon dioxide absorption bands. The detector is a nitrogen-cooled mercury-cadium-telluride (MCT) detector. All data were taken with the sample at room temperature.

Figure 6 shows the Michelson interferometer in the optical bench of the FTIR and the locations of the different ports on the integrating sphere. The reflectance sample port is located opposite the entrance port where the incoming radiation beam undergoes its first internal reflection. The radiation impinging on the sample is broken into three components with respect to the plane of the sample—that scattered into the forward hemi-

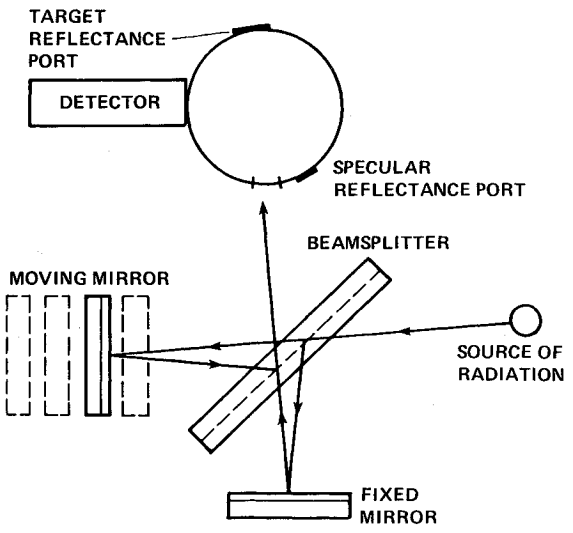

Fig. 6 Experimental setup showing the optical bench and the positions of reflectance and transmittance ports on integrating sphere.

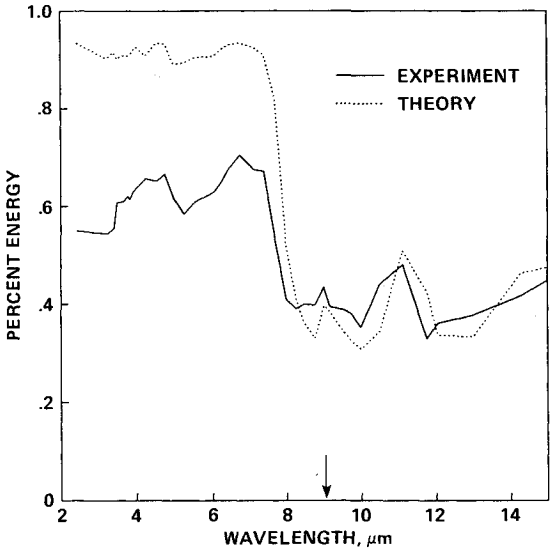

Fig. 7 Experimental and theoretical results assuming random spacing, for 9 μm diam silica fibers, for forward scattering.

sphere, into the backward hemisphere, or absorbed by the material. The location of the scatterer at the entrance or at the reflectance port determines which components of the scattered energy are collected by the sphere and measured by the detector after multiple internal reflections.

The fibers in the sample holder covered a width of 0.58 mm, as measured from a photograph. The entrance port of the integrating sphere is 19 mm in diameter. In order to increase the fraction of energy in the incident beam incident on the fibers, the beam was passed through a 1×10 mm slit. This increased the ratio of the area covered by the fibers to the incident beam from approximately 0.04 to 0.6. The effect of the slit on the measurement system was compensated for by increasing the sensitivity of the detector and the number of scans and by running a background correction with the slit in place.

Results

Experimental measurements of the transmittance through and reflectance from the parallel quartz fibers of the sample are presented in Figs. 7 and 8 along with theoretical predictions of the forward and backward scattering made by assuming a random distribution of the fibers, using Eq. (13a). Experimental measurements were made at 450 data points, but the theoretical calculations were made at 40 discrete wavelengths from which the indices of refraction and absorption were available. The experimental measurements corresponding to the 40 wavelengths were extracted from the data base for comparison with the theoretical predictions.

The measured transmittance T is the sum of the directly transmitted energy and the energy scattered into the forward direction by the fibers. The theoretical transmittance is given by

$$T = (1 - b/B) + b/B$$

$$(1 - Q_{aN} - Q_{sN,\text{for}} - Q_{sN,\text{back}} + Q_{sN,\text{for}})$$

$$= 1 + (b/B)(-Q_{aN} - Q_{sN,\text{back}}) \qquad (15)$$

where Q_e is the extinction efficiency, Q_a the absorption efficiency, and $Q_{s,\text{for}}$ and $Q_{s,\text{back}}$ are the efficiencies of scattering by the fibers in the forward and backward hemispheres. The cross-sectional area of the beam is represented by B and that of the fibers is b.

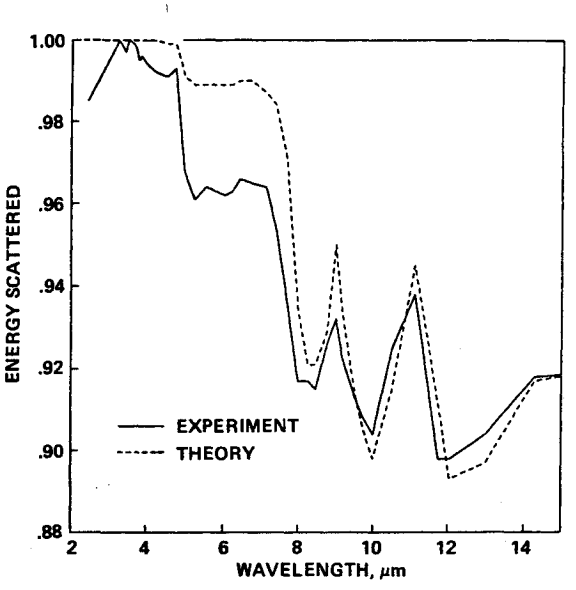

Fig. 8 Experimental and theoretical results assuming random spacing, for 9 μm diam silica fibers, for total scattering.

Transmittance measurements were made with the fibers in the sample holder normal to the beam of incident radiation at the entrance port of the sphere. Figure 7 shows the experimentally measured transmittance and the theoretical predictions for scattering using Eq. (13a) over the range from 2.5 to 15 μm. Equation (13a) is used since the fibers in the experiment were not perfectly coplanar but were bunched together. All the wavelengths at which the local maxima and minima occur are well predicted by the theory. At larger wavelengths, the agreement between the measured and the predicted values is seen to be extremely good: the root mean square deviation between the corresponding measured and predicted values is 0.03 for the data points at wavelengths greater than 8 μm. This is approximately equal to the fiber diameter of 9 μm, which corresponds to a size parameter of π. At shorter wavelengths, the size parameter grows to a relatively large value, and the agreement between the theory and experiment is not as close. The root mean square deviation in this case is 0.22. Since the

theoretical predictions agree qualitatively with the experimental data, the data can in fact be well correlated over the entire measurement range by the following empirical expression

$$T = 0.67 + 0.28(-Q_{aN} - Q_{sN,\,\text{back}}) \tag{16}$$

resulting in a very small root mean square deviation of 0.041.

Figure 8 shows the measured total scattering by the fiber array in the midinfrared range from 2.5 to 15 μm, compared to the theoretical predictions assuming the fibers to be randomly spaced. The measurements were made with the fibers 1 mm in front of the diffuse reflectance target at the sample reflectance port shown opposite the entrance port in Fig. 6. The impinging radiation is either scattered backward directly into the sphere, scattered forward to the diffuse reflector, which then in this case scatters it back into the sphere, or absorbed by the material. Only the energy absorbed by the material is lost to the sphere, i.e., not received by the detector. The ratio of the areas of the fibers to the beam gives the percent of the incident radiation subject to either absorption or scattering. The beam is 7 mm in diameter at this location. The total energy scattered in this case is given by

$$S = 1 - (b/B)Q_{aN} \tag{17}$$

where Q_a is the absorption efficiency, which is calculated assuming the fibers are randomly spaced. As seen in Fig. 7, the experimental data verifies the validity of the theoretical model for wavelengths greater than 8 μm, i.e., when the size parameter α is not a large quantity. At shorter wavelengths or larger α, the theory agrees qualitatively with the measurements showing local maxima and minima at the same wavelengths, but it does not give the very good quantitative agreement seen for longer wavelengths. In both cases, however, the agreement is very close, showing a root mean square difference of 0.014 at the smaller wavelengths and 0.0048 at the longer wavelengths.

The close agreement between the data and the theory at the longer wavelengths defines the limit of applicability for the theory to size parameters α less than approximately π. This result is as anticipated since the assumption in Eq. (2) that the phase change across the fiber is negligible breaks down for large size parameters. At large size parameters, i.e., small wavelengths, the incident radiation sees one fiber not as a discrete scattering object but as a collection of scattering centers. The N fibers no longer correspond to N scatterers; therefore the idealized geometry and the straightforward summation over N scatterers is no longer valid.

Summary and Conclusions

Theoretical considerations developed in this paper indicate that the scattering characteristics of a system of parallel fibers is affected by the location of the fibers with respect to each other. The mechanism of interference of the scattered waves from different fibers has been ignored in the classical formulations of scattering theory of fibrous systems. The present theoretical framework analyzes this effect, and the resultant model incorporates these interference effects. The theoretical results indicate that the scattering efficiency for randomly positioned fibers is reduced from that predicted from independent scattering theory. Experimental results for coplanar, randomly positioned fibers confirm these theoretical predictions.

The analysis presented here is limited to the case of energy being incident normal to the axes of a collection of parallel fibers. At oblique incidence, interference between scattered waves from different incident polarizations occurs and is therefore more complicated to model. Similar cross polarization interference is present when fibers are placed perpendicularly to each other in the same plane even though the incident energy may be normal to the plane. Another perceived limitation of the analysis is that it does not experimentally agree at large size parameters. This could be attributed to the fact that as the size parameter becomes large, the Mie theory used in computing the phase function may not be an accurate representation of the scattering, and instead diffusely reflecting fibers must be considered, which would yield a very different scattering diagram. Mie theory, which considers smooth walls at all wavelengths, yields a very forward scattering phase function whereas a diffuse fiber in the geometrical limit is highly backward scattering with forward scattering due to diffraction only.

References

[1]Pitts, W.C., and Murbach, M.S., "Thermal Design of Aero-assisted Orbital Transfer Vehicle Heat Shields for a Conical Drag Brake," *Journal of Spacecraft and Rockets*, Vol. 23, No. 4, July 1986, pp. 442–448.

[2]Walberg, G.D., "A Review of Aerobraking for Mars Missions," IAF Paper 88-196, Oct. 1988.

[3]Covington, M.A., and Sawko, P.M., "Optical Properties of Woven Ceramic Fabrics of Flexible Heat Shields," AIAA Paper 86-1281, June 1986.

[4]Kerker, M., *The Scattering of Light and Other Electromagnetic Radiation,* Academic, New York, 1961.

[5]Kumar, S., and Tien, C.L., "Dependent Scattering and Absorption of Radiation by Small Particles," *Proceedings of the ASME/AIChE 24th National Heat Transfer Conference (Pittsburgh)*, HTD Vol. 72, 1987, pp. 1–7; also *Journal of Heat Transfer*, Vol. 112, Feb. 1990, pp. 178–185.

[6]Drolen, B.L., Kumar, S., and Tien, C.L., "Experiments on Dependent Scattering of Radiation," AIAA Paper 87-1485, June 1987.

[7]Kumar, S., and Tien, C.L., "Effective Diameter of Agglomerates for Radiative Extinction and Scattering," *Combustion Science and Technology*, Vol. 66, Dec. 1989, pp. 199–216.

[8]Bohren, C.F., and Huffman, D.R., *Absorption and Scattering of Light by Small Particles,* Wiley-Interscience, New York, 1983.

[9]Wang, K. Y., Kumar, S., and Tien, C. L., "Radiative Transfer in Thermal Insulations of Hollow and Coated Fibers," *Journal of Thermophysics and Heat Transfer,* Vol. 1, No. 4, 1987, pp. 289–295.

[10]Lee, S.C., "Radiation Heat Transfer Through Fibers Oriented in Planes," AIAA Paper 87-1487, June 1987.

[11]Debye, P., "Note on the Scattering of X-Rays," *Journal of Mathematics and Physics,* Vol. 4, March 1925, pp. 133–147.

[12]Cartigny, J.D., Yamada, Y., and Tien, C.L., "Radiative Transfer with Dependent Scattering by Particles: Part 1—Theoretical Investigation," *Journal of Heat Transfer*, Vol. 108, Sept. 1986, pp. 608–613.

[13]Palik, E.D., ed., *Handbook of Optical Constants of Solid*, Academic, New York, 1985, pp. 749–763.

[14]Touloukian, Y.S., and DeWitt, D.P., *Thermophysical Properties of Matter*, Vol. 8, *Thermal Radiative Properties of Nonmetallic Solids*, Plenum Press, New York, 1972, Fig. 144.

[15]Driscoll, W.G., ed., *Handbook of Optics*, Optical Society of America, McGraw-Hill, New York, 1978, Secs. 7–25.